05,08

Magnetic Characteristics and Bloch Coefficients in $Sr_2Fe_{1-x}Mo_{1+x}O_{6-\delta}$ Films

© D.A. Kiselev[1], S.S. Starukhina[1], A.S. Bykov[1], A.V. Petrov[2], A.G. Yudenkov[3], N.A. Kalanda[2,¶]

[1] National University of Science and Technology „MISiS“,
Moscow, Russia
[2] Scientific and Practical Materials Research Center, „National Academy of Sciences of Belarus“,
Minsk, Belarus
[3] State Center „Belmicroanalysis“ of the Scientific-Technical Center of JSC „INTEGRAL“,
Minsk, Belarus

¶ E-mail: kalanda@physics.by

Received August 20, 2025
Revised August 20, 2025
Accepted October 14, 2025

In this work, the modes of obtaining single-phase $Sr_2Fe_{1-x}Mo_{1+x}O_{6-\delta}$ films obtained by the ion-beam sputtering method have been developed and their magnetic characteristics were investigated. It was found that the dependence of magnetization on temperature $M(T)$, measured in a magnetic field of 0.1 T, does not obey the Bloch law for any of the studied films. Its description required the use of Dyson corrections taking into account the contribution of magnons with large wave vectors. It was found that for the composition of films with an excess of iron and with its deficiency, the value of B (Bloch coefficient) increases with an increase in the superstructural ordering of Fe/Mo (P) cations B. At the same time, in the films of the $Sr_2Fe_{1.2}Mo_{0.8}O_{6-\delta}$ composition, with an increase in P, the thermal stability is lower than in films of the $Sr_2Fe_{0.9}Mo_{1.1}O_{6-\delta}$ composition, whereas with a decrease in P — it is vice versa. It has been shown that by controlling the composition and synthesis modes of films of the compositions $Sr_2Fe_{1.2}Mo_{0.8}O_{6-\delta}$ and $Sr_2Fe_{0.9}Mo_{1.1}O_{6-\delta}$, it is possible to control the value of B, and hence the thermal stability of the spin polarization of the entire system.

Keywords: double perovskites, ion beam deposition, magnetic characteristics, antistructural defects, Bloch coefficients.

DOI: 10.61011/PSS.2025.10.62635.239a-25

1. Introduction

Modern spintronics is in demand of materials with stable spin polarization at room temperature to fabricate the non-volatile memory devices, sensors, neuromorphic computing elements, and logic gates. The promising candidate is the double perovskite Sr_2FeMoO_6 which is featuring semi-metallic properties, high Curie temperature ($T_C \sim 420-450$ K) and a 100 % spin polarization in theory [1–6].

The key factor explaining the properties of Sr_2FeMoO_6, is the degree of the super-structural ordering of Fe and Mo cations. The antisite defects $[Fe_{Mo}]/[Mo_{Fe}]$ and various degrees of oxidation of $(Fe^{2+}/Fe^{3+}/Fe^{4+})$ and $(Mo^{4+}/Mo^{5+}/Mo^{6+})$ cations destroy any further ordering leading to lower spin polarization and worsening of magnetic characteristics.

In thin films [7,8], the sensitivity to defects increases due to oxygen vacancies, interfacial stresses, and cationic nonstoichiometry. One of the methods for controlling properties is to vary the composition in $Sr_2Fe_{1-x}Mo_{1+x}O_6$ system, which allows adjusting the magnetic order and suppress any antisite defects [8].

Among the ways to control the properties is variation of the composition in $Sr_2Fe_{1-x}Mo_{1+x}O_6$ system. The variation in x parameter allows adjusting the magnetic ordering, charge states of cations (ratios of Fe^{3+}/Fe^{2+} and Mo^{5+}/Mo^{6+}), coercive force and Curie temperature [3,4], and also suppress the antisite defects. However, to prevent the formation of impurity phases, precise control of the composition during film growth is necessary [7].

Of practical interest are the films of $Sr_2Fe_{1.2}Mo_{0.8}O_{6-\delta}$ ($SF_{1.2}M_{0.8}O$) and $Sr_2Fe_{0.9}Mo_{1.1}O_{6-\delta}$ ($SF_{0.9}M_{1.1}O$). The composition with an excess of Fe exhibits increased saturation magnetization, and with an excess of Mo, it exhibits better cationic ordering. However, the synthesis of such films requires precision control due to the tendency to formation of impurity phases (e. g., $SrMoO_4$, $SrFeO_3$ or iron oxides), which radically impair the functional properties of the material [7,8]. Therefore, to obtain high functional properties in $Sr_2Fe_{1-x}Mo_{1+x}O_6$ films it is required to provide a precision control of the composition, improve the growth modes and make a comprehensive analysis of the defective structure.

The industrial use of materials in spintronics devices requires high reproducibility of their physical-chemical characteristics, which directly depends on the degree of spin polarization of charge carriers, which can be purposefully controlled by monitoring the superstructural ordering of Fe/Mo cations in double perovskites and the value of the

Bloch coefficient. This parameter serves as an important tool for modeling and predicting the functionality of promising devices, from the magnetic random access memory (MRAM) in smartphones and high-efficiency spin-voltaic cells for solar cells to qubits and interfaces in quantum computers [9].

Based on the above, the purpose of this work is to study the effect of the superstructural ordering of cations on the magnetic properties and parameters of Bloch's law in the nonstoichiometric thin films $Sr_2Fe_{1-x}Mo_{1+x}O_6$ for control of their spin polarization and getting the reproducible characteristics necessary in the spintronics applications.

2. Methods for preparation and study of samples

The films of $Sr_2Fe_{1.2}Mo_{0.8}O_{6-\delta}$ ($SF_{1.2}M_{0.8}O$) and $Sr_2Fe_{0.9}Mo_{1.1}O_{6-\delta}$ ($SF_{0.9}M_{1.1}O$) with a thickness of about $\sim 1\,\mu$m were deposited by method of the ion-plasma sputtering in vacuum system Z-400 („Leybold-Heraeus") equipped with an oil-free pumping system based on a turbomolecular pump. The target films of $SF_{1.2}M_{0.8}O$ and $SF_{0.9}M_{1.1}O$, 50 mm in diameter and 5 mm thick were used as a sputtered material. The chamber of the vacuum installation was equipped with a flanged two-beam ion source with a closed electron drift based on an accelerator with an anode layer and a magnetron sputtering system. A special feature of the ion source is the ability to generate two independent ion beams, one of which is used to sputter the target material, and the other to clean the substrates. The substrates were preliminarily cleaned with an ion beam. The chamber of the vacuum unit was evacuated to a residual pressure of 10^{-3} Pa. Ar was supplied to the ion source to the level of pressure $2.0 \cdot 10^{-2}$ Pa. The purification time, ion energy, and discharge current were constant in all experiments and were, respectively, 3 min, 700 eV, 40 mA. The consumption of work gases was controlled using automatic gas flow regulators RRG-1. The targets were sputtered with the help of argon (ions energy 1250 eV, current 65 mA) on the polycore substrates (Al_2O_3), providing chemical inertness and high adhesion to the films of $Sr_2Fe_{1-x}Mo_{1+x}O_{6-\delta}$ system. The residual argon pressure in the gas chamber was $5 \cdot 10^{-2}$ Pa. The temperature of the substrate, according to the technical capabilities of the installation, was 670 K. The thickness of the deposited films was measured on different sections of the witness films using an MII-4 interferometer and adjusted by changing the time of layer deposition.

The films were additionally annealed in the flow of gas mixture (Ar, 1 % H_2/Ar, 3 % H_2/Ar and 5 % H_2/Ar) in the temperature chambers with temperature regulation using RIF-101 regulator and temperature monitoring using Pt−Pt/Rh(10 %) thermocouple with an accuracy of ± 0.5 K.

The phase composition of films and the degree of superstructural ordering of iron and molybdenum cations (P, %) were determined based on the analysis of diffraction patterns obtained using DRON-3 system in CuK_α-emission using dataset„ICSD-PDF2" (Release 2000), and „POWDERCELL" and „FULLPROF" software [10,11].

The grains' microstructure and morphology were studied using metallographic microscope „OLYMPUS GX-41", as well as by using the method of scanning electron microscopy on „Hitachi S-4800". The temperature dependences of the films magnetization were studied on a general-purpose unit „Cryogenic Limited" within the range 4.2−300 K, in magnetic field 0.1 T, with an accuracy of no more than 2 %.

3. Experimental findings and their discussion

The structural perfection of thin films $Sr_2Fe_{1-x}Mo_{1+x}O_{6-\delta}$ synthesized by ion beam deposition (IBD) requires careful optimization of a number of interrelated technological parameters, including deposition rate, temperature of the post-growth annealing of films and partial pressure of oxygen. The benefit of IBD method is the possibility of forming a dense film at relatively low temperatures, which helps to reduce the number of defects [7,8]. The deposition rate plays a key role in the formation of the film microstructure. The optimal speed ensures a uniform distribution of small grains in the films, which is benign for their magnetic properties [8]. A two-stage strategy seems to be the best choice: the initial low speed leads to formation of a buffer layer between the film and the substrate to improve the adhesion and reduce the stress at the „film-substrate" interface. The subsequent high deposition rate reduces the time required for sputtering and increases the uniformity of the main part of the film [7]. The deposition rate when the film thickness is up to 20 nm was 2 nm/min; with a further increase in the film thickness to 1 μm, the rate increased to 18 nm/min.

When studying the structure and microstructure of $SF_{1.2}M_{0.8}O$ and $SF_{0.9}M_{1.1}O$ films, the formation of the structure of double perovskite and other phases was not detected, that is, the films are amorphous, have a specular a black surface with no grains in them (Figure 1).

The high deposition rate in the second stage causes the atoms/molecules to precipitate too quickly. They do not have enough time and energy (obtained from the substrate or during secondary processes) for effective surface diffusion, search for energetically advantageous positions (growth points) and the formation of large crystallites. As a result, a process of random „freezing" prevails. This mechanism effectively suppresses the segregation of the components of a complex compound, since atoms of different types, deposited almost simultaneously, „freeze" in-situ without any possibility of diffusion and formation of regions enriched in one element or another. Rapid deposition captures nonequilibrium states and structural defects. These factors contribute to the formation of metastable solid

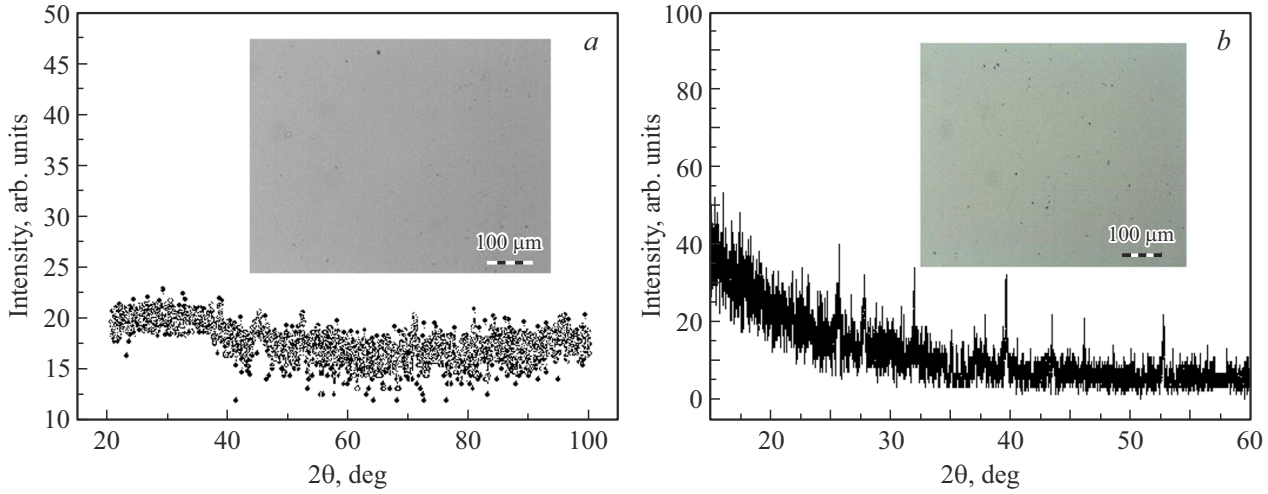

Figure 1. X-ray diffraction patterns of $SF_{1.2}M_{0.8}O$ (*a*) and $SF_{0.9}M_{1.1}O$ films (*b*), deposited in two steps. The deposition rate when the film thickness is up to 20 nm was 2 nm/min; with a further increase in the film thickness to 1 μm, the rate increased to 18 nm/min. The following tabs show the microstructure of films obtained by optical microscopy.

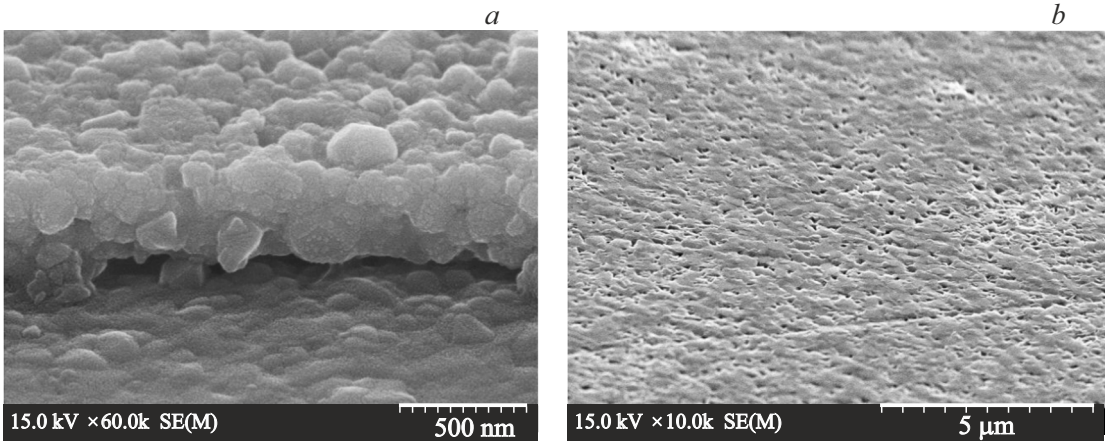

Figure 2. Images obtained using scanning microscopy; the microstructures of $SF_{1.2}M_{0.8}O$ (*a*) and $SF_{0.9}M_{1.1}O$ (*b*) films deposited in two stages. The films were deposited at the second stage with 12 nm/min, followed by annealing at 1173 K for 1 h in an argon stream.

solutions or amorphous phases that have good nanoscale homogeneity, but no thermodynamic equilibrium. As a result, the high deposition rate significantly increases the density of defects in the deposited material.

To structure the films and reduce the number of defects, they were subjected to post-growth heat treatment in an inert medium and a reduction in the deposition rate at the second stage to 12 nm/min. A series of experiments showed that the optimal mode is annealing at $T = 1173$ K for 1 h, in an argon stream. According to scanning electron microscopy data, the films of $SF_{1.2}M_{0.8}O$ and $SF_{0.9}M_{1.1}O$ were porous, with a developed surface pattern and weak adhesion to the substrate (Figure 2). According to the obtained X-ray diffraction data the films were characterized by phase inhomogeneity: in $SF_{1.2}M_{0.8}O$ sample the additional phases $SrFeO_3$ and $SrMoO_4$ were found (Figure 3, *a*), and in $SF_{0.9}M_{1.1}O$ sample, along with the main phase of the double perovskite, the impurity of $SrMoO_4$ was found (Figure 3, *b*). The main phase in the films of both compositions was a double perovskite having tetragonal symmetry (spatial group $I4/m$).

The coefficient of superstructural ordering of Fe and Mo cations turned out to be low. For the film of $SF_{0.9}M_{1.1}O$ it was $P \approx 58\,\%$, which indicates high concentration of the antisite defects $[Fe_{Mo}]$ and $[Mo_{Fe}]$ at a level of $n \approx 21\,\%$. In $SF_{1.2}M_{0.8}O$ film no superstructural ordering was observed ($P \approx 0\,\%$) and $n \approx 25\,\%$. These microstructural features, namely, the phase inhomogeneity of the films and the high concentration of antisite defects, may have an adverse effect on their magnetic properties, which requires further improvement of the conditions for their fabrication.

Reducing the deposition rate in the second stage to 8 nm/min and increasing the film thickness to 3 μm, followed by annealing at $T = 1173$ K for 1 h in a stream

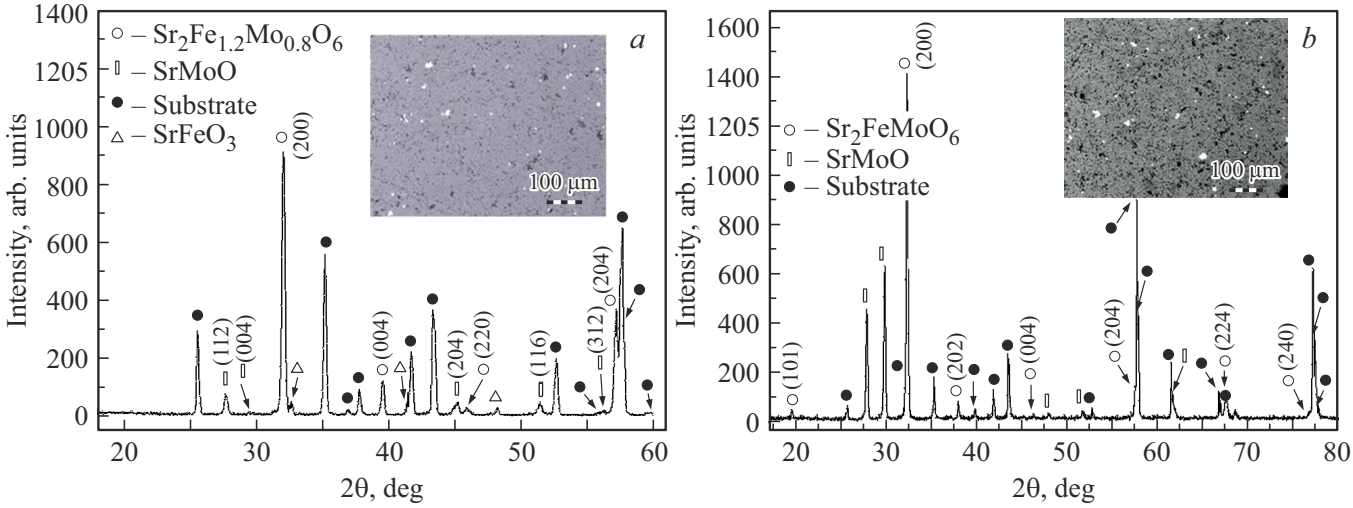

Figure 3. X-ray diffraction patterns of $SF_{1.2}M_{0.8}O$ (*a*) and $SF_{0.9}M_{1.1}O$ films (*b*), deposited in two steps. During the second stage the films were deposited with a rate of 12 nm/min, followed by annealing at 1173 K for 1 h in an argon stream. The following tabs show the microstructure of films.

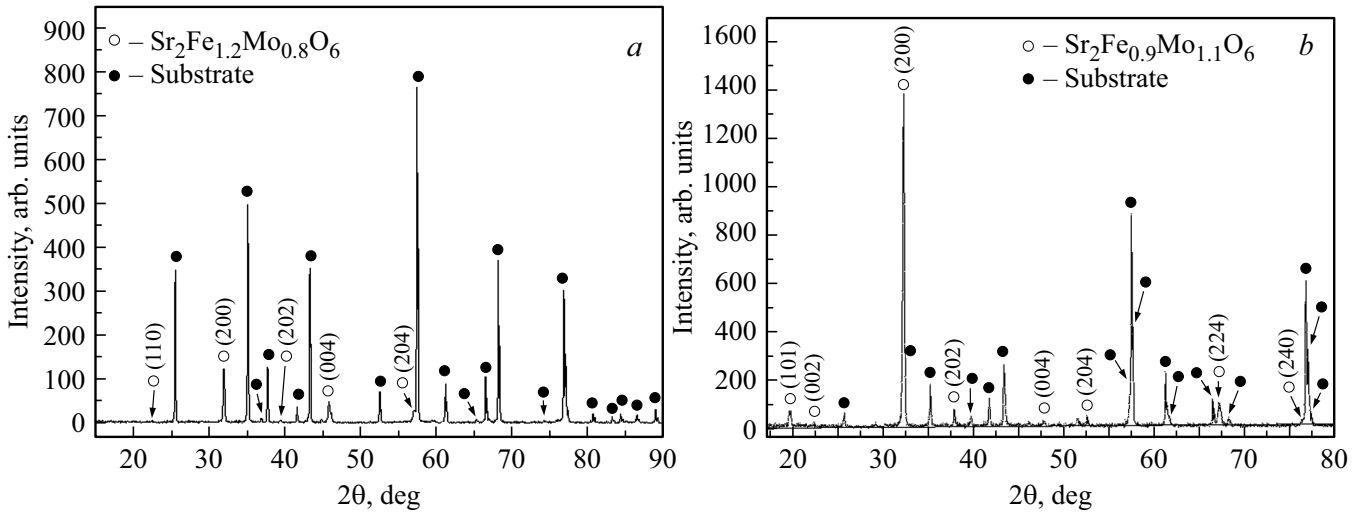

Figure 4. X-ray diffraction patterns of $SF_{1.2}M_{0.8}O$ (*a*) and $SF_{0.9}M_{1.1}O$ films (*b*), deposited in two steps. The films were deposited at the second stage with a rate of 8 nm/min followed by annealing at $T = 1173$ K for 1 h in the stream of inert gases 1 % H_2/Ar.

of an inert gas mixture of 1 % N_2/Ag led to single-phase films $SF_{0.9}M_{1.1}O$, and lower concentration of the antisite defects $n \approx 18$ % at $P \approx 64$ %. At the same time, single-phase behavior is also observed in $SF_{1.2}M_{0.8}O$ films, while superstructural ordering is absent ($P \approx 0$ %), Figure 4. When studying the microstructure of films, an increase in their density, adhesion, and a decrease in the roughness of the surface relief is observed (Figure 5).

A comparative analysis of the magnetic properties of the obtained films revealed that $SF_{1.2}M_{0.8}O$ and $SF_{0.9}M_{1.1}O$ films are characterized by different saturation magnetization values M_s (Figure 6). At a temperature of 10 K and a magnetic field applied along the film plane the saturation magnetization was $M_s \sim 1.8\,\mu_B$/f.u. for $SF_{1.2}M_{0.8}O$ film and $M_s \sim 2.47\,\mu_B$/f.u. for $SF_{1.1}M_{0.9}O$.

These values are below the theoretically predicted value $M_{\text{theory}} = 4\,\mu$B/f.u. [4]. At that, the coercive force was $\mu_0 H_c = 0.031$ T for $SF_{1.2}M_{0.8}O$ film and $\mu_0 H_c = 0.018$ T for $SF_{0.9}M_{1.1}O$ film.

Lower saturation magnetization of $SF_{1.2}M_{0.8}O$ film is caused by higher concentration of antisite defects ($[Fe_{Mo}]$ and $[Mo_{Fe}]$), compared to $SF_{0.9}M_{1.1}O$ films. These defects disrupt the cationic ordering of Fe/Mo, change the orientation of strongly hybridized $4d\,t_{2g}$ — orbitals of cations Mo^{5+} ($S = 1/2$) and $3d$ ($t_{2g}^3 e_g^2$) — orbitals of cations Fe^{3+} ($S = 5/2$), which suppresses the ferrimagnetic ordering between the sublattices of Fe and Mo [3–5]. Moreover, in conditions of oxygen deficiency ($\delta > 0$) part of cations Fe^{3+} ($3d^5$) may reduce to Fe^{2+} ($3d^6$), which in the octahedral crystalline field Fe^{2+}, are, generally, in the high-spin state

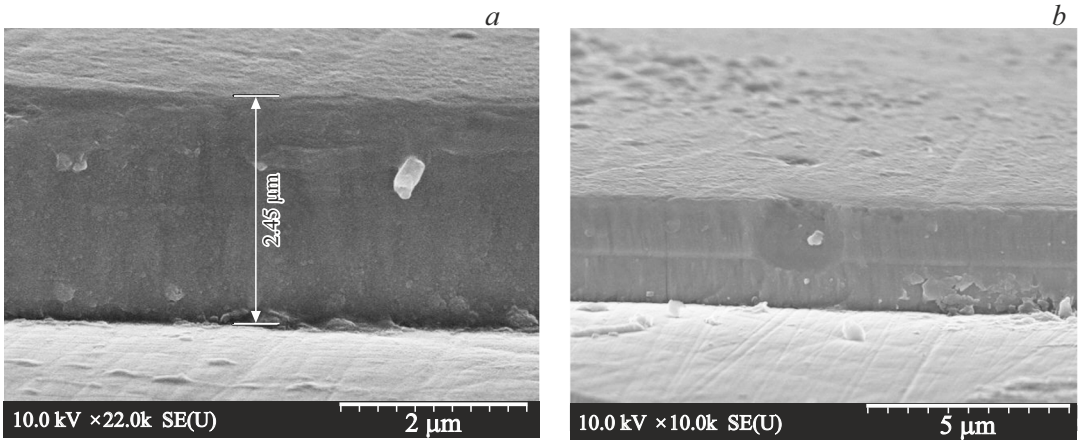

Figure 5. Scanning electron microscopy images of $SF_{1.2}M_{0.8}O$ (*a*) and $SF_{0.9}M_{1.1}O$ (*b*) films, deposited in two stages. The films were deposited at the second stage with a rate of 8 nm/min followed by annealing at $T = 1173$ K for 1 h in the stream of inert gases 1 % H_2/Ar.

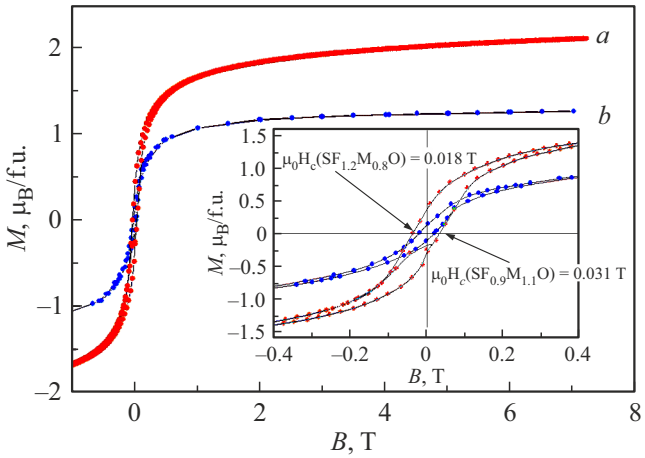

Figure 6. Field dependencies of magnetization of $SF_{0.9}M_{1.1}O$ (*a*) and $SF_{1.2}M_{0.8}O$ (*b*) films deposited during the second stage at a rate of 8 nm/min followed by annealing at $T = 1173$ K for 1 h in the stream of inert gases 1 % H_2/Ar.

($t_{2g}^4 e_g^2$, $S = 2$). The appearance of Fe^{2+} ions promotes the formation of clusters of Fe^{2+}–O^{2-}–Fe^{2+} type, in which the hyper-exchange interaction is antiferromagnetic, according to the Goodenough–Kanamori– Andersen rules [12]. Thus, the structure of $SF_{1.2}M_{0.8}O$ film may contain both antisite defects and antiferromagnetic clusters based on Fe^{2+}, which together contributes to the formation of a magnetically inhomogeneous structure that increases the coercive force [7,8]. $SF_{0.9}M_{1.1}O$ films are characterized by a more uniform magnetic structure compared to $SF_{1.2}M_{0.8}O$, which is proved by higher saturation magnetization M_s and lower $\mu_0 H_c$ for compositions with an excess of molybdenum compared with films containing an excess of iron (Figure 6). To raise the superstructural ordering of Fe/Mo cations the films $SF_{1.2}M_{0.8}O$ and $SF_{0.9}M_{1.1}O$ were subjected to the post-growth annealing at $T = 1173$ K for 1 h in a stream of inert gases 3 % H_2/Ar and 5 % H_2/Ar. As seen from the XPA data, $SF_{1.2}M_{0.8}O$ films annealed in the mixture of inert gases 3 % H_2/Ar had $P = 62$ %, and the films annealed in the mixture of inert gases 5 % H_2/Ar had $P = 74$ %. While $SF_{0.9}M_{1.1}O$ films annealed in the mixture of inert gases 3 % H_2/Ar had $P = 72$ %, and annealed in the mixture of inert gases 5 % H_2/Ar had $P = 80$ %.

Since Bloch law is the physical basis for modeling, predicting, and implementing the functions of today's devices, it is reasonable to consider the dependence of its parameters on the composition and superstructural ordering of Fe/Mo cations in $Sr_2Fe_{1-x}Mo_{1+x}O_{6-\delta}$ films both with an excess of iron ($x > 0$) and with its deficiency ($x < 0$). The temperature dependence of magnetization in $SF_{1.2}M_{0.8}O$ and $SF_{0.9}M_{1.1}O$ films is described by Bloch law. Its behavior with increasing temperature is determined by the complex interaction of magnetic sublattices, structural defects, and thermal fluctuations. The main regularities include the following: in the low-temperature region, with the rise of temperature, a violation of the magnetic ordering occurs due to the excitation of magnons (spin waves). For acoustic magnons with dispersion $E(k) \sim k^2$, their number increases proportionally to $T^{3/2}$, which leads to a decrease in magnetization. In this case, the temperature dependence of the magnetization, according to Bloch law is expressed as:

$$M(T) = M(0)(1 - BT^{3/2}), \qquad (1)$$

where $M(0)$ is maximum magnetization of the films, B is the Bloch constant, which is a fitting parameter that characterizes the contribution of magnon excitations to magnetization decline.

It was found that the best approximation according to Bloch law of the dependence $M(T)$, measured in an external magnetic field 0.01 T, was observed in the temperature range $4.2 < T < 110$ K (Figure 7). The adjusting coefficients are given in Table 1. In $SF_{1.2}M_{0.8}O$ and $SF_{0.9}M_{1.1}O$ films the antisite defects ($[Fe_{Mo}]$ and $[Mo_{Fe}]$) compromise

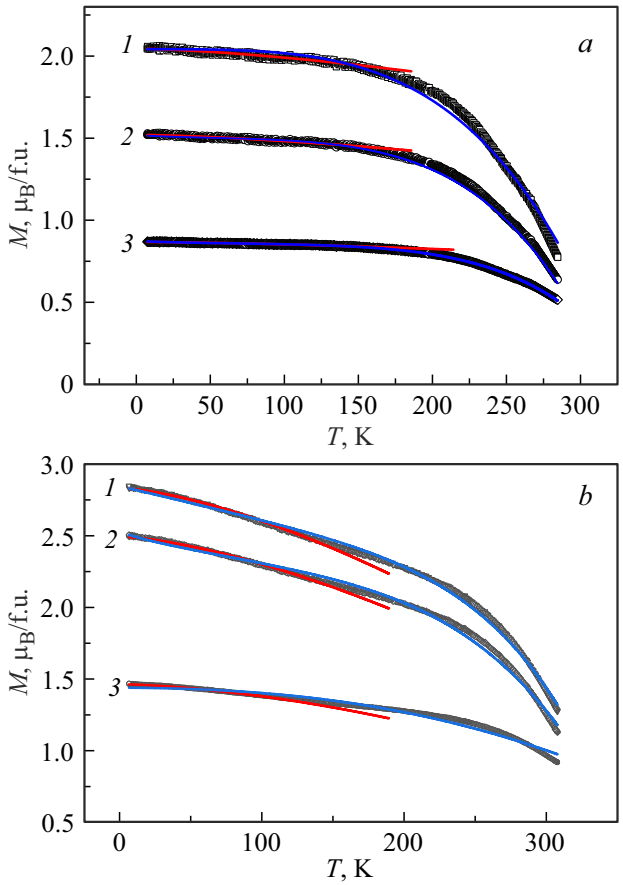

Figure 7. Temperature dependencies of magnetization for $SF_{1.2}M_{0.8}O$ films (*a*), with a superstructural ordering of cations Fe/Mo $P = 0\,\%$, $P = 62\,\%$ and $P = 74\,\%$ for curves (*3*), (*2*) and (*1*), respectively, and for $SF_{0.9}Mo_{1.1}O$ (*b*) films with $P = 64\,\%$, $P = 72\,\%$ and $P = 80\,\%$ for curves (*3*), (*2*) and (*1*), respectively, measured in the external magnetic field 0.1 T. Black lines — experimental data; red lines — experimental data approximated by function (1); blue lines — experimental data approximated by function (2).

the ideal ordering of Fe^{3+} ($S = 5/2$) and Mo^{5+} ($S = 1/2$) sublattices. This enhances the scattering of spin waves, increasing B and accelerating the decline in magnetization.

An increase in temperature above 150 K leads to the excitation of magnons with large wave vectors **k**, for which the dispersion law deviates from the quadratic one, as well as to a more intense interaction between the magnons.

To account for these effects, Bloch law needs to be corrected. In the Dyson model [13], this deviation is described by adding the term $CT^{5/2}$:

$$M(T) = M_0(1 - BT^{3/2} - CT^{5/2}), \qquad (2)$$

where B and C — positive constants. The term $CT^{5/2}$ is related to the consideration of the non-quadratic law of dispersion and magnon interactions. The obtained approximations (1) and (2) of $SF_{1.2}M_{0.8}O$ and $SF_{0.9}Mo_{1.1}O$ films are given in Tables 1 and 2.

Table 1. The adjusting coefficients obtained by approximating the temperature dependence of the magnetization of $SF_{1.2}M_{0.8}O$ films by various functions

	Value	Error
Approximation of the temperature dependence of magnetization using function $M(T) = M(0)(1 - BT^{3/2})$		
$P \sim 74\,\%$		
$M(0)$	2.04492	$4.48746 \cdot 10^{-4}$
B	$2.66253 \cdot 10^{-5}$	$2.56302 \cdot 10^{-7}$
R^2	0.9374	
$P \sim 62\,\%$		
$M(0)$	1.52008	$3.11629 \cdot 10^{-4}$
B	$2.48737 \cdot 10^{-5}$	$2.39733 \cdot 10^{-7}$
R^2	0.9422	
$P \sim 0\,\%$		
$M(0)$	0.86803	$1.24652 \cdot 10^{-4}$
B	$1.74234 \cdot 10^{-5}$	$1.68798 \cdot 10^{-7}$
R^2	0.9371	
Approximation of the temperature dependence of magnetization using function $M(T) = M(0)(1 - BT^{3/2} - CT^{5/2})$		
$P \sim 74\,\%$ $M(T) = M(0)(1 - BT^{3/2} - CT^{5/2})$		
$P \sim 74\,\%$		
$M(0)$	2.04191	0.09548
B	$3.11 \cdot 10^{-5}$	$2.14 \cdot 10^{-7}$
C	$2.71 \cdot 10^{-7}$	$1.24 \cdot 10^{-8}$
R^2	0.9907	
P 62 %		
$M(0)$	1.52296	0.05829
B	$2.42 \cdot 10^{-5}$	$7.52 \cdot 10^{-8}$
C	$2.19 \cdot 10^{-7}$	$1.02 \cdot 10^{-8}$
R^2	0.9943	
$P \sim 0\,\%$		
$M(0)$	0.87661	0.01359
B	$7.86 \cdot 10^{-6}$	$4.21 \cdot 10^{-8}$
C	$1.19 \cdot 10^{-7}$	$6.42 \cdot 10^{-9}$
R_2	0.9981	

Table 2. The adjusting coefficients obtained by approximating the temperature dependence of magnetization of $SF_{0.9}Mo_{1.1}O$ films by various functions

	Value	Error
Approximation of the temperature dependence of magnetization using function $M(T) = M(0)(1 - BT^{3/2}$		
$P \sim 80\,\%$		
$M(0)$	2.83249	$3.21 \cdot 10^{-4}$
B	$8.09 \cdot 10^{-5}$	$2.51 \cdot 10^{-7}$
R^2	0.9687	
$P \sim 72\,\%$		
$M(0)$	2.49409	$2.86 \cdot 10^{-4}$
B	$77 \cdot 10^{-5}$	$2.54 \cdot 10^{-7}$
R^2	0.9711	
$P \sim 64\,\%$		
$M(0)$	1.4643	$2.42 \cdot 10^{-4}$
B	$5.25 \cdot 10^{-5}$	$1.14 \cdot 10^{-7}$
R^2	9.9721	
Approximation of the temperature dependence of magnetization using function $M(T) = M(0)(1 - BT^{3/2} - CT^{5/2})$		
$P \sim 80\,\%$		
$M(0)$	2.83249	$3.21 \cdot 10^{-4}$
B	$2.04 \cdot 10^{-5}$	$1.04 \cdot 10^{-4}$
C	$2.44 \cdot 10^{-7}$	$1.22 \cdot 10^{-8}$
R^2	0.9877	
$P \sim 72\,\%$		
$M(0)$	2.54613	$2.92 \cdot 10^{-4}$
B	$1.33 \cdot 10^{-5}$	$8.69 \cdot 10^{-8}$
C	$2.24 \cdot 10^{-7}$	$1.17 \cdot 10^{-8}$
R^2	0.9843	
$P \sim 64\,\%$		
$M(0)$	1.43937	$1.17 \cdot 10^{-4}$
B	$9.02 \cdot 10^{-6}$	$5.91 \cdot 10^{-8}$
C	$1.65 \cdot 10^{-7}$	$8.21 \cdot 10^{-9}$
R^2	0.9889	

Calculated Bloch constants for $SF_{1.2}M_{0.8}O$ films, taking into account the Dyson correction $B = (3.11-0.786) \cdot 10^{-5}\,K^{-3/2}$, and for $SF_{0.9}Mo_{1.1}O$ films $B = (2.04-0.902) \cdot 10^{-5}\,K^{-3/2}$ practically correspond to the values found by other authors (e. g., $7.03 \cdot 10^{-5}\,K^{-3/2}$ for $Sr_2FeMoO_{5.5}S_{0.5}$ [14]; $5.9 \cdot 10^{-5}\,K^{-3/2}$ for $Fe_{29}Hi_{49}P_{14}B_6Si_2$ [15]). The close values of the obtained results with other authors can be related using a good fit, according to the expression (2) with a coefficient of determination ($R^2 > 0.98$) (see Tables 1, 2).

When considering the dependence of the Bloch constant on the parameter P, it was noted that both for the films with an excess of iron and with its deficiency, the value B increases with the rise in Fe/Mo cations superstructural ordering. The growth of B means that the material more easily loses its magnetization (and, consequently, spin polarization) when heated, which is bad for the thermal stability of electronic devices. Whereas in $SF_{1.2}M_{0.8}O$ films with the rise of P, according to the data from Tables 1 and 2, the thermal stability is lower than in $SF_{0.9}Mo_{1.1}O$ films while with the decline in P — vice versa. Thus, by controlling the composition and synthesis modes of $SF_{1.2}M_{0.8}O$ and $SF_{0.9}Mo_{1.1}O$ films we may control the value B, and, hence, the stability of spin polarization.

4. Conclusion

The following conclusions may be drawn from the above-mentioned results:

– due to improvement of deposition modes the single-phase films were synthesized $Sr_2Fe_{1.2}Mo_{0.8}O_{6-\delta}$ ($SF_{1.2}M_{0.8}O$) and $Sr_2Fe_{0.9}Mo_{1.1}O_{6-\delta}$ ($SF_{0.9}M_{1.1}O$) having improved structural characteristics and different superstructural ordering of Fe/Mo cations. For this, a two-stage sputtering was used, with a decreased rate in the second stage from 18 to 8 nm/min and subsequent annealing at 1173 K for 1 h in various mixtures of inert gases;

– the study of magnetic properties revealed the inhomogeneous magnetic structure of all films. This behavior is explained by two main factors: the presence of antisite defects that destroy the ordering at the nodes of the crystal lattice and suppress ferrimagnetic ordering, as well as under conditions of oxygen deficiency ($\delta > 0$), some of the cations $Fe^{2+}(3d^5)$ can be restored to $Fe^{2+}(3d^6)$, which in the octahedral crystal field, Fe^{2+} are usually in a high-spin state ($t_{2g}^4 e_g^2$, $S = 2$). The appearance of Fe^{2+} ions promotes the formation of clusters of $Fe^{2+}-O^{2-}-Fe^{2+}$ type in which the hyperexchange interaction is antiferromagnetic, according to the Goodenough–Kanamori–Andersen rules. Thus, the structure of $SF_{1.2}M_{0.8}O$ film may contain both antisite defects and antiferromagnetic clusters based on Fe^{2+}, which together contributes to the formation of a magnetically inhomogeneous structure that increases the coercive force;

– it was found that the dependence of magnetization on temperature $M(T)$, measured in a magnetic field of 0.1 T, does not obey the Bloch law (does not approximate with $R^2 \to 100\,\%$) for any of the studied films. Its description

required the application of Dyson corrections, which take into account the contribution of magnons with large wave vectors. It was noted that both for the films with an excess of iron and with its deficiency, the value B increases with the rise in Fe/Mo cations' superstructural ordering. Moreover, in $SF_{1.2}M_{0.8}O$ films, with an increase of P, the thermal stability is lower than in $SF_{0.9}Mo_{1.1}O$ films, whereas with a decrease in P, on the contrary. Thus, by controlling the composition and synthesis modes of $SF_{1.2}M_{0.8}O$ and $SF_{0.9}Mo_{1.1}O$ films, it is possible to control the value of B, and, hence, the thermal stability of spin polarization.

Funding

The study was performed within State Research Program 1.1.1 of the Republic of Belarus „Materials science, new materials and technology", Subprogram „Condensed state physics and development of new functional materials and production technologies" („Physics and Technology of Materials"), project BRFFI No. F24V-005, as well as supported by grant of the Russian Science Foundation No. 24-19-00729, https://rscf.ru/project/24-19-00729.

Conflict of interest

The authors declare that they have no conflict of interest.

References

[1] D.D. Sarma. Curr. Opin. Solid State Mater. Sci. **5**, *4*, 261 (2001).
[2] T. Fix, A. Barla, C. Ulhaq-Bouillet, S. Colis, J.P. Kappler, A. Dinia. Chem. Phys. Lett. **434**, 276 (2007).
[3] D. Serrate, J.M. DeTeresa, M.R. Ibarra. J. Phys. Condens. Matter. **19**, 1 (2007).
[4] M. Yarmolich, N. Kalanda, S. Demyanov, H. Terryn, J. Ustarroz, M. Silibin, G. Gorokh. Beilstein J. Nanotechnol. **7**, 1202 (2016).
[5] G. Suchaneck, N. Kalanda, E. Artiukh, M. Yarmolich, N.A. Sobolev. J. Alloys Compd. **860**, 158526 (2021).
[6] S.E. Demyanov, A.V. Petrov. FTT **64**, 1788 (2022). (in Russian).
[7] G. Suchaneck, N. Kalanda, E. Artsiukh, G. Gerlach. Phys. Status Solidi B **257**, 1900312 (2020).
[8] N.A. Kalanda, S.E. Demyanov, A.V. Petrov, D.V. Karpinsky, M.V. Yarmolich, S.K. Oh, S.C. Yu, D.-H. Kim. J. Electron. Mater. **45**, 3466 (2016).
[9] Y. Shao, P. Kh. Amiri. Adv. Mater. Technol. **8**, 2300676 (2023).
[10] W. Kraus, G. Nolze. J. Appl. Crystallogr. **29**, 301 (1996).
[11] J. Rodríguez-Carvajal. Commission on powder diffraction (IUCr). Newsletter **26**, 12 (2001).
[12] C. Ritter, M.R. Ibarra, L. Morellon, J. Blasco, J. Garcia, J.M. De Teresa. J. Phys. Condens. Matter. **12**, 8295 (2000).
[13] F.J. Dyson. Phys. Rev. **102**, 1230 (1956).
[14] G. Huo, X. Ren, L. Qian, N. Zhang, S. Liu, X. Yuan. J. Magn. Magn. Mater. **343**, 119 (2013).
[15] S.M. Bhagat, M.L. Spano, K.V. Rao. J. Appl. Phys. **50**, 1580 (1979).

Translated by T.Zorina